Advanced lab course for Bachelor's students

M21 Medical physics
Positron Emission Tomography (PET)

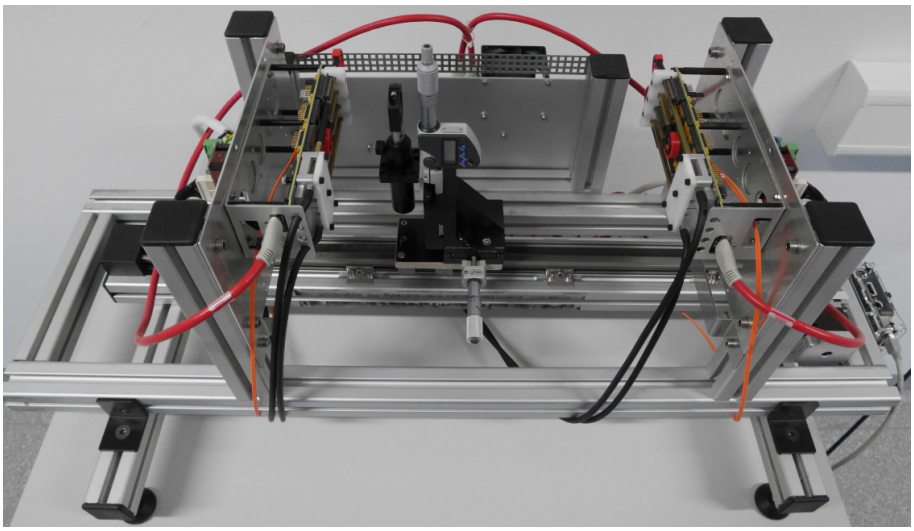

January 2017

Thomas Dey, email: thomas.dey@pmi.rwth-aachen.de

Prerequirements:

- Interaction of gamma rays and matter
- Scintillators
- Photo diodes, p-n-junctions
- Radiation detection

Aims of this experiment:

- Detector electronics
- Digital Silicon Photo-Multipliers
- Determination of detector characteristics
  - Energy resolution
  - Timing resolution
  - Detector sensitivity

Contents

1 Preface

Aim of this lab course is to show the principle of positron emission tomography (PET) imaging and how digital Silicon-Photo-multipliers (dSiPM) are used in this application. You will perform experiments to determine the sensitivity, the energy and timing resolution as important characteristics of a PET scanner. Measurements are performed on a simple PET scanner consisting of 2 detector elements, measuring γ events of a ^{22}Na-point source.
These instructions are organized as follows: In the first two sections the principle of PET imaging (2.1) and gamma detection with (digital) SiPM (2.2) are briefly described. In Section 2.3 the PET scanner characteristics that will be measured in this lab course, are explained as well as their influence on imaging.
The experimental setup and procedure are delineated in sections 3.1 and 3.2. Finally instructions for the data analysis are given in section 3.3.
The experiment will be conducted in the rooms of the Physics of Molecular Imaging Systems (PMI) department at the Zentrum für Bio-Medizintechnik (ZBMT), first floor, Pauwelstr. 17, 52074 Aachen. Please ring the bell of the PMI institute at the front door to get entrance to the ZBMT.

Figure 1.1: Directions to ZBMT Aachen, (Google Maps link).

2 Theoretical Background

2.1 Principle of PET-Imaging

In contrast to computed tomography (CT) and magnetic resonance imaging (MRI), both imaging patient's anatomy, the aim of positron emission tomography (PET) is to show metabolic functions. Figure 2.1 gives an overview of the molecular sensitivity (lowest concentration of an imaged agent that can be accurately detected in a medium) and spatial resolution of different imaging modalities.
In PET, a small amount of a radioactively-labeled chemical compound (so-called tracer) is injected in the patient. The tracer binds to targeted molecules and allows imaging of the desired metabolic process e. g. glucose uptake of tumor cells to identify cancer metastasis. PET aims to image the spatial and temporal distribution of the tracer, showing the biological process(es) and ideally allowing also quantification e. g. to evaluate therapy response. Clinically, it is used mainly in the fields of oncology, cardiology and neurology e. g. for the diagnosis of Alzheimer's disease.
Tracers for PET imaging are positron emitters like ^{18}F-fluorodeoxyglucose (FDG) and ^{82}Rb-chloride. The emitted positron deaccelerates until it either annihilates directly with an electron or after forming a bound state with an electron (called positronium). In both cases, the annihilation results usually in two γ photons of 511 keV emitted back to back (at an angle of 180°) in the center-of-mass frame.
What angles between the two γ photons, are observed in the lab frame?
Ideally, the emitted γ photons travel through the patient and are detected by the PET-detector surrounding the patient. The points of detection define a so-called line of response (LOR), on which the annihilation has occurred (see Figure 2.2(a)). By measuring a large amount of these LORs, the original tracer distribution can be calculated (see Figure 2.2(b)). The calculation of the underlying tracer distribution from the detected events or LORs is called (image) reconstruction. Frequently used reconstruction method are filtered back-projection or maximum likelihood expectation maximization. More information regarding image reconstruction methods can be found in [3, 4, 6].
By measuring the time difference between the detection of the two photons, the line of response can be limited to a smaller section and ideally to a single point (see Figure 2.3). The width of the time difference distribution of a point-like source is called coincidence resolving time (CRT), usually displayed as full width at half maximum (FWHM). In reality, the CRT of PET-systems is in the order of 200-500 ps. The timing uncertainty is mainly caused by the scintillation process, but also timing jitter of the electronics contributes to the CRT (about 20 ps). In this lab course the

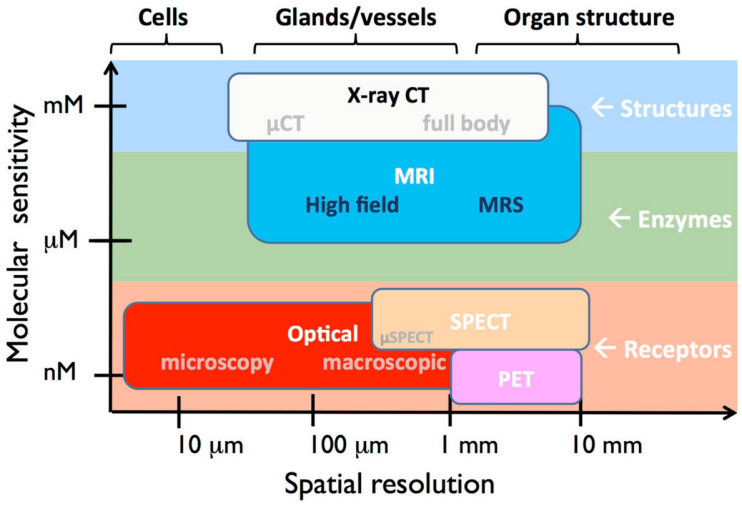

Figure 2.1: Comparison of medical imaging modalities with respect to molecular sensitivity and spatial resolution, from [7]

timing resolution of the PET scanner will be measured and used to determine the unknown position of a point source.

2.2 Detection of gamma photons by silicon photo-multipliers

2.2.1 Scintillators for PET-imaging

In PET imaging usually the γ-photons are detected in a two-staged process. First, a γ-photon is converted to a large number of optical or ultraviolet photons by scintillation. In a second step these (optical) photons are detected by photo-sensors. Since the principle of scintillation is already described in the instructions of the lab course T1 [1], it is not repeated here. Instead the properties of scintillators that are important for PET-imaging are delineated.

Attenuation coefficient at 511 keV. The linear attenuation coefficient is the fraction of attenuated incident photons per unit thickness of a material. A high attenuation coefficient at 511 keV reduces the probability that those γ-photon passes the scintillator without depositing (its total) energy and potentially leaves undetected or are detected with a wrong energy value.

Intrinsic energy resolution is a lower bond for the detector energy resolution (see Section 2.3.1). Energy resolution is important to distinguish photons emitted at the point of annihilation from those that have been scattered (e. g. by Compton scattering in the patient). Scattered photons partly loose the information about the annihilation point and lead to false LORs causing additional

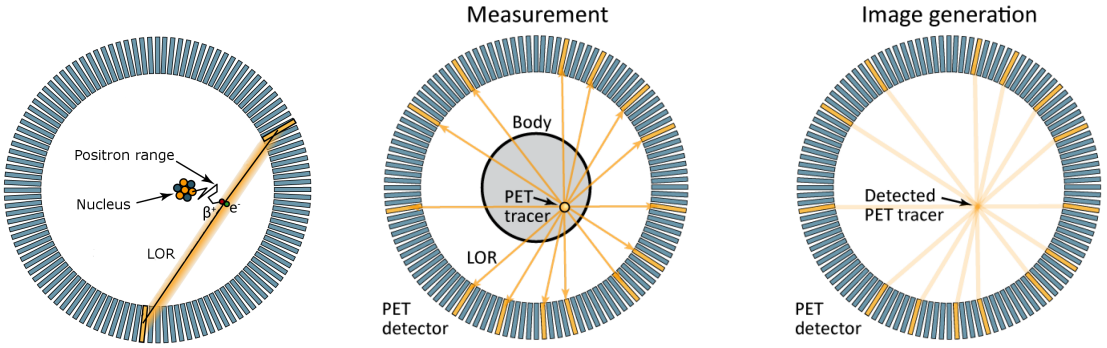

(a) Positron annihilation and LOR definition, modified from [9]

(b) PET measurement and image generation, from [9]

Figure 2.2: Visualization of PET imaging principle.

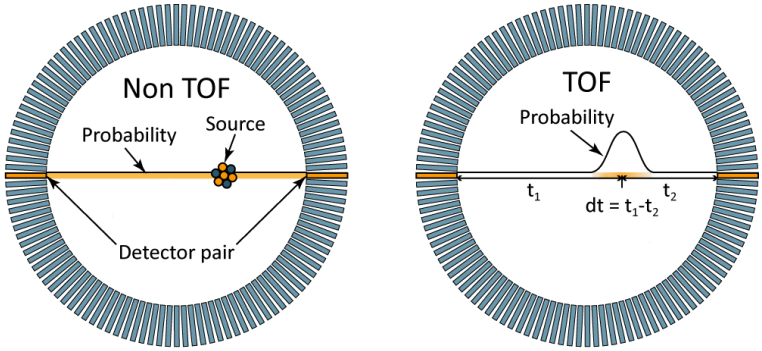

Figure 2.3: Visualization of the Tof-PET principle, modified from [9]

noise in the reconstructed image. The role of energy resolution and effects of scatter are described in more details in Section 2.3.1. To achieve a good energy resolution, a high light output with a small variation in the number of produced photons per energy is required.

Fast emission of photons is required to allow exact time stamping of the energy deposit in the scintillator, which is obviously needed to allow time-of-flight measurements. Furthermore, a short decay time reduces the probability that scintillation processes of multiple γ photons pile-up, what makes it difficult or impossible to determine the number of incident γ photons.

Scintillator materials commonly used in PET imaging are crystals of bismuth germanium oxide ($Bi_4Ge_3O_{12}$, BGO) or cerium-doped lutetium yttrium orthosilicate ($Lu_{1.8}Y_{0.2}SiO_5(Ce)$, LYSO). The relevant properties of BGO, LYSO and for comparison also the properties of sodium iodide (NaI) are given in table Table 2.1.
The optical photons emitted in the scintillator have to traverse and leave the scintillator material to be detected by the photo sensors. Therefore, the scintillator has

Parameter	NaI	BGO	LYSO
Effective Z	50.6	73	65
Density / (g/cm^3)	3.67	7.13	7.1
Peak emission / nm	410	480	420
Light output / ph.	19400	4200	~ 16000
Intrinsic $\Delta E/E(\%)$	5.8	3.1	~ 9
Decay time / ns	230	300	~ 40
Index of refraction	1.85	2.15	1.8
Attenuation coefficient / (cm^{-1})	0.34	0.96	0.82

Table 2.1: Scintillator properties, if not stated otherwise for a gamma energy of 511 keV. The properties largely depend on the exact doping and production of the scintillators and are not to be taken as exact values (taken from [5]).

to be transparent for these photons and total reflection at the boundary surface of the scintillator and the photo detector has to be avoided. Hence, also the refractive index of the scintillation material is an important property.
Regarding the assembly of scintillator material in PET detectors, there are basically three options(see Figure 2.4):

One-to-one coupling The scintillator material is cut in blocks with a base area equal to the size of the photon detector elements and is directly glued on top of these. So one photo detector element is coupled to a scintillator 'pixel'. This is the simplest configuration, but is just feasible for relatively large scintillator pixels of a few millimeter.

High-resolution scintillator In this configuration the scintillator elements have a much smaller base area than the photo detector elements. The optical photons are distributed to the photo detectors via an extra layer (so-called light guide). The light guide spreads the light of a scintillator element to multiple photo detector elements. Therefore, serveral photo detector elements have to be read-out and a positioning algorithm is required to determine the crystal hit by the γ-photon (see Figure 2.5).

Monolithic crystal For a monolithic crystal, the position of the interaction of the γ-photon with the scintillator material has to be reconstructed from the photo detector signal. This requires knowledge of the correlation of the scintillation position and the measured signals, which has to be derived by calibration measurements.

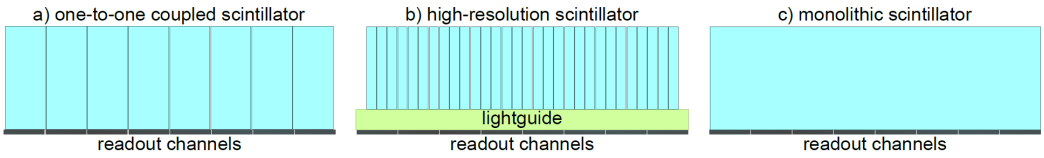

Figure 2.4: Scintillator crystal configurations, from [5]

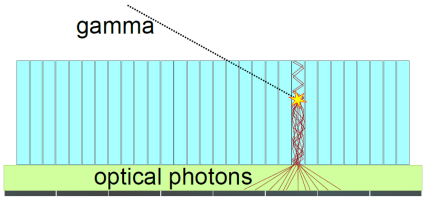

Figure 2.5: Sketch of a high resolution scintillator configuration, [5]

2.2.2 Photo-detectors

For the detection of the optical photons, emitted by the scintillator, usually two different kinds of detectors are used: Photo-multipliers and semiconductor-based sensors. Here, we focus on semiconducting photo sensors, particularly digital Silicon-Photomultipliers (dSiPM).
To explain the principle of a dSiPM, we introduce a photo diode as the basic implementation of a semiconductor-based photo sensor. First, we consider a photo diode as a simple p-n-junction. More information on p-n junctions and their properties can be found in the instructions of T1 [1].
If a photon with a sufficient energy (higher than the band gap) hits the depletion zone, an electron hole pair is created. Due to the intrinsic voltage the electron travels to the cathode (n-doped layer), while the hole travels to the anode (p-doped layer), resulting in a so-called photo-current. To increase the (sensitive) depletion zone, an additional low-doped layer (so-called the intrinsic region) is often incorporated between the p- and n-layers resulting in a so-called PIN-diode (see Figure 2.6).
By a reverse bias voltage the depletion width is also increased, while the response time of diode is reduced. However, the reverse bias also results in a temperature dependent leakage current, which is present even in the absence of light (dark current). If the reverse bias voltage is below the breakdown voltage, the photo-current is proportional to the number of absorbed photons and only slightly depending on the bias voltage. However, since each photon creates only a single electron-hole pair the photo-current is very small.
For bias voltages higher than the breakdown voltage, each free charge carrier in the depletion zone induces an avalanche of charged particles. The rise time of the resulting signal is in the order of a few picoseconds and due to the internal gain, the photo-current is much higher compared to a PIN-diode. However, in this so-called

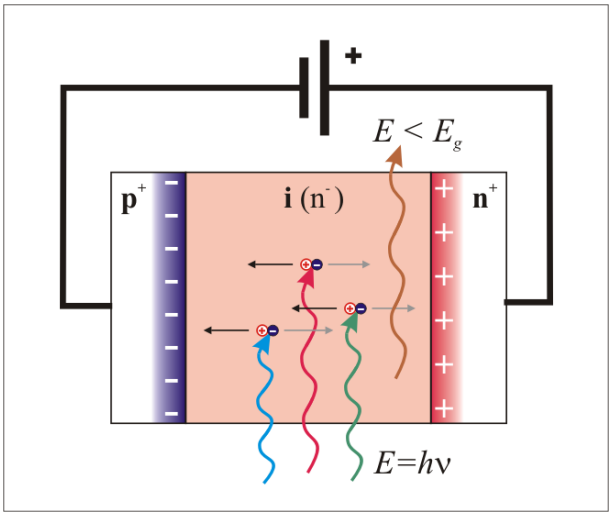

Figure 2.6: PIN-photodiode with space charge distribution under reverse voltage. (@User:Kirnehkrib/Wikimedia Commons/ CC BY SA 3.0)

Geiger mode[1] the avalanche is the same for every event and no longer proportional to the number of incident photons. Therefore, such a device, called single photon avalanche diode (SPAD), delivers a binary signal if one or more photons are detected.
Since the avalanches in a SPAD are self-sustaining, quenching is required to reset a SPAD after photo detection. For quenching the bias voltage has to be reduced below the breakdown voltage. This can be done passively by a high ohmic resistor in series with a SPAD. The photo-current leads to a voltage drop at the resistor reducing the bias voltage below the breakdown voltage and hence stopping the avalanche. After quenching, the bias voltage recovers. This recovery process takes about a few nanoseconds and during this period no further photons can be detected. To reduce this dead time, the bias voltage can also be reduced actively by electronics (active quenching). In this case the SPAD has to be reset by ramping-up the bias voltage again to make the SPAD sensitive for the next photon.
To build a useful photo counting sensor, a Silicon Photomultiplier (SiPM), multiple small area SPADs or microcells are combined and parallel connected (see Figure 2.7). The photo-currents of the SPADs add up to a signal from which the number of detected photons can be recovered by pulse height or shape analysis. The digitization and time stamping of the analog SPAD signals is done by an application-specific integrated circuit (ASIC). Figure 2.8 shows a light detection system consisting of SPADs and a ASIC-based readout electronics.
In digital SiPMs (dSiPM) each SPAD signal is digitized, transforming a single SPAD into a digital device. These digital signals are more robust than the analog-signal-summation in analog SiPMs, which is prone to temperature-induced gain changes and usually requires compensation. The better robustness is particular interesting

[1]The name is inspired by the analogy to the Geiger Müller counter

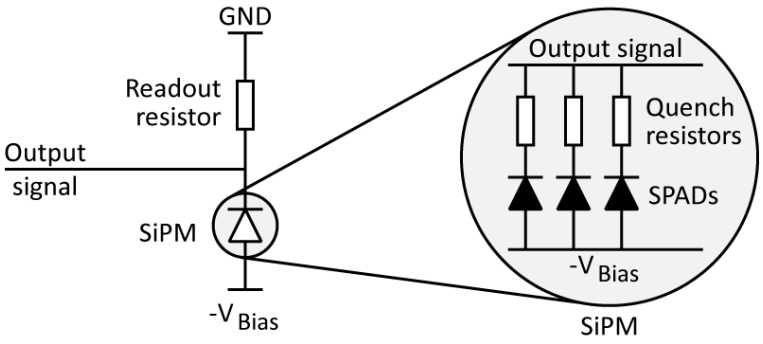

Figure 2.7: SiPM circuits: An SiPM is constructed from SPADs in series with individual quench resistors, connected in parallel (right). In series with a readout resistor, they produce an analog output signal. Taken from [9].

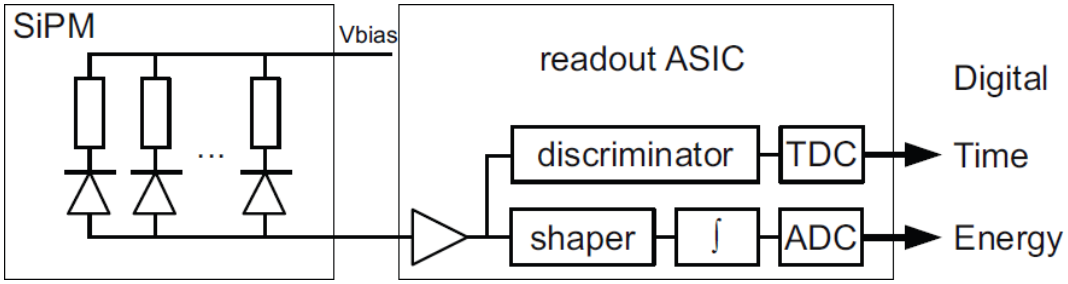

Figure 2.8: Scintillation light detector systems based on an analog silicon photomultiplier. (reprinted from Frach et al. [2], ©IEEE)

for the combination of PET detectors and MRI, since the inside of an MRI is a very harsh environment for electronics, due to the strong static magnetic field and potential induction of high voltages by time-varying magnetic fields.
Since each SPAD can be actively quenched the dead time due to quenching is reduced, which is important to avoid pile-up of multiple events in case of high count rates. Furthermore, selective deactivation of those SPADs, that due to impurities or defects show the highest trigger probability, can reduce the number of events caused by the noisy dark-current, the so-called dark count rate (DCM) significantly.

2.2.3 Single and Coincidence processing

The detected optical photons are grouped to reconstruct single interactions of γphotons in the scintillator (singles). As described in Section 2.1 two coincident events are required to determine the LORs needed for reconstruction of the tracer distribution. Hence, the individual singles have to be checked for coincidence with other events. For this purpose a sliding coincidence window is used to find coincident singles. Only coincidences of exactly two singles are accepted, others are rejected.

2.3 PET scanner characteristics

The scanner characteristics covered in this lab course are: energy resolution, timing resolution and sensitivity. In the following these characteristics, their influence on imaging and how they can be measured are delineated.

2.3.1 Energy resolution

The 511 keV photons traveling through the patient interact with patient's tissue mainly via the mechanisms of photoelectric effect and Compton scattering. Since the mean free path of 511 keV in water is about 70 mm, in clinical applications most photons are scattered. Compton scattering alters the energy and direction of the scattered photon, therefore scattered photons lead to wrongly assumed LORs resulting in background noise in the image (see Figure 2.9).

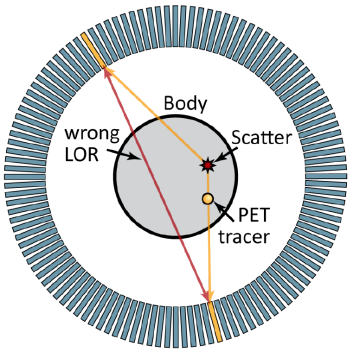

Figure 2.9: Scattered gamma photons result in wrongly assumed LORs that increase the image background noise, from [9]

By filtering these scattered photons by their reduced energy, this background noise can be avoided or reduced. However, the limited energy resolution broadens the photo peak at 511 keV and depending on the energy resolution an energy window of sufficient width has be chosen to preserve a sufficient sensitivity. In Figure 2.10 measured energy spectra are depicted. Figure 2.10(a) shows the spectrum of detected singles while Figure 2.10(b) shows the spectrum of single events that are in coincidence with another event. The energy resolution of a PET scanner is usually defined by the FWHM of the 511 keV photo peak over the energy. To evaluate the role of energy resolution, the relation between maximum scatter angle and energy resolution can be derived from Compton formula (Equation 2.1) and is plotted in Figure 2.11.

$$E'_\gamma = \frac{E_\gamma}{1 + \frac{E_\gamma}{m_0 c^2 (1 - \cos\theta_c)}} \tag{2.1}$$

Here, E_γ is energy of the incident photon, E'_γ is the energy of the photon after the scattering process, m_0 is the rest electron mass, and θ_c is the scattering angle.

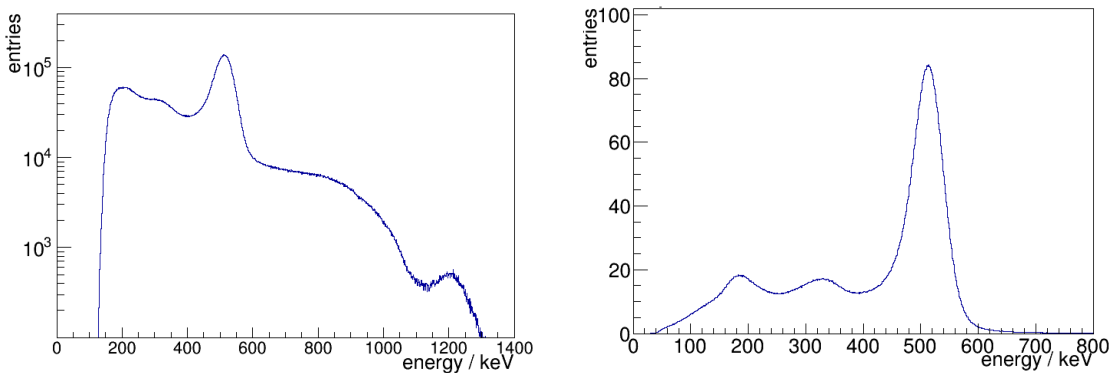

(a) Single energy spectrum of a ^{22}Na point source.

(b) Energy spectrum of coincident singles of a ^{18}F-filled line source.

Figure 2.10: Energy spectra of singles and conincident singles, from [5]

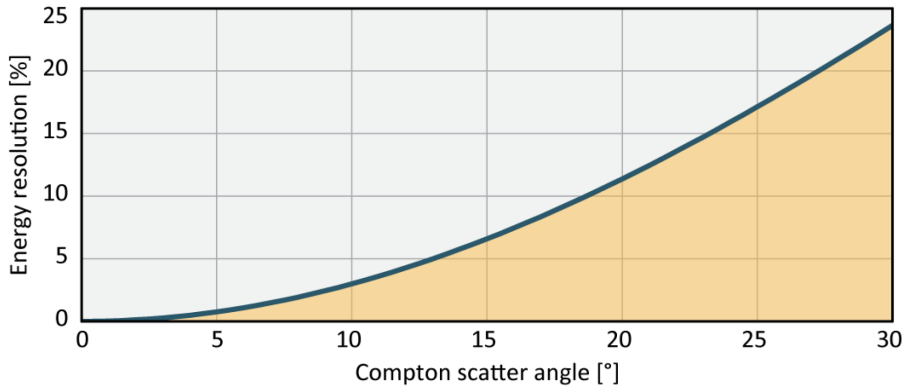

Figure 2.11: Energy resolution that is needed to detect that a 511 keV photon was Compton-scattered, over the scatter angle (and respectively: the Compton scatters that can be detected, relative to the energy resolution).Taken from [9]

To measure the energy resolution of the PET-detector an energy calibration has to be performed first (see [5] for detailed information). After calibration a spectrum of coincident singles is acquired and the energy resolution can then be derived by fitting a Gaussian distribution to a suitable part of the photo peak. The linearity of the calibration can be checked by the second photo peak of ^{22}Na at 1275 keV acquired in the energy spectrum of all singles.

Besides scatter inside the patient, what other processes can cause detection of photons with less than 511 keV?

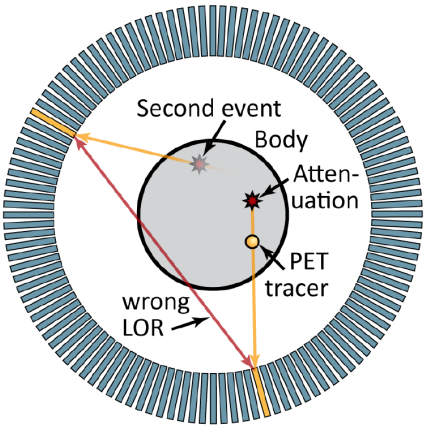

Figure 2.12: Random coincidence: Two single γ-photons of different events (the others are e. g. attenuated or the second event was outside the FOV) are detected simultaneously as a wrong LOR.b Taken from [9]

2.3.2 Timing resolution

To combine detected single γ photons to coincident events, a sliding time window is used to group singles to coincidences. The size of this coincidence window (CW) has to be chosen large enough to allow the γ photons to travel through the complete distance between the detectors plus a safety margin depending on the timing resolution of the detector. On the other hand a large CW can result in the situation that γ photons of different annihilations are falsely group to coincidences. Considering an example with two annihilations in a CW, the following cases are possible:

More than two photons detected In this case the events can be discarded, or further processing is required to find the most probable LOR(s), which might lead to wrong LORs, of course.

Two photons detected If two photons leave the detector undetected, the detector cannot distinguish this situation from detecting a true coincidence, therefore a wrong LOR is assumed in this case. These events are called randoms and induce background noise to the image. Fig 2.12 illustrates the situation for random events. The random rate is approximately proportional to the length of the coincidence window.

Timing resolution of a PET scanner can be determined by acquiring a time difference histogram of a point source and fitting a Gaussian distribution it (see Figure 2.13). Usually the timing resolution is reported as the FWHM of the fitted Gaussian distribution.
If the timing resolution is smaller than the time that the photons need to pass the distance between the detectors, time of flight (ToF) measurements become useful. In this case the timing difference can be used to limit the LORs to smaller sections and ideally to a single point (see Figure 2.3). In reality, the timing resolution is

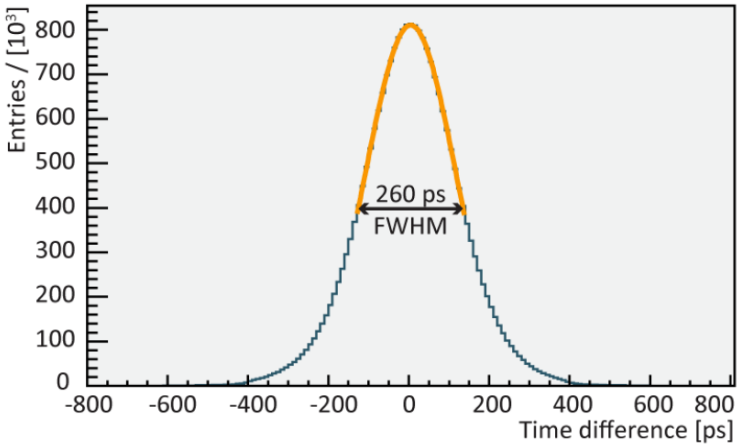

Figure 2.13: Timing resolution measured with the Hyperion-IID PET-insert using timing-optimized settings. A single ^{22}Na point source (1.3 MBq) was placed in the center of the FOV for the scan. Taken from [9]

in the order of 200-500 ps FWHM, so the LORs are limited to a length of 6-15 cm. ToF-imaging results in less noise and therefore a better contrast in the images.
In this lab course also the unknown position of a point source has to be determined by time of flight measurements.
Make a rough estimation of the error of this measurement.

2.3.3 Sensitivity

The sensitivity is a measure for the fraction of radioactive decays that are detected by the system. The sensitivity depends on a number of efficiencies and settings:

Geometric Efficiency Only those γ photons have the chance to deposit energy in the scintillator and be detected that pass the scintillating material at least partly. Accordingly, the geometric efficiency is defined as the solid angle covered by the detector.

Detection Efficiency Even if a γ photon travels through the scintillator, it might not deposit energy and leave undetected. A scintillator material with high attenuation (at 511 keV) and also larger scintillators can reduce the rate of undetected photons. However, large scintillators induce other problems in PET imaging.
What problems can be caused by large scintillator crystals?

Dead Time If a SPAD has detected a photon, it has to be read-out and reset to be sensitive for the next event. Photons hitting this microcell during this period cannot be detected and therefore are lost. This reduces the sensitivity in particular in case of high count rates.

The dark count rate described in section 2.2.2 has also an influence on the sensitivity. In case of a dark noise event the microcell has to be read-out and reset, leading to additional dead time. Although these noise events can be filtered-out by a trigger logic, the dead time results in a loss of sensitivity.
To measure the sensitivity a weak point source is placed in the center position between the detectors. The sensitivity is then determined as the ratio of the coincidence count rate divided by the rate of β-decays of the source.

3 Setup and Procedure of the Measurements

3.1 Setup

3.1.1 General Setup

The general setup of the experiment is depicted in Fig. 3.1. The actual detector consists of two module boards, called single processing unit (SPU) see Figure 3.2(a). The SPUs can hold up to six detector stacks. In the current experiment two of these stacks are mounted per SPU. An detector stack consists of an interface board, the actual sensor board, a light guide and a scintillator mounted on top (see Figure 3.2(b)). The SPUs are responsible for controlling the sensor boards, e. g. enabling or disabling SPADs or ramp-up the bias voltage. In addition, they manage the data transmission of PET data to the data acquisition and processing server (DAPS). A third module board (so-called backbone) provides sync and reference clock to the SPU. These signals are conducted via HDMI connections between each SPU and the backbone.
The SPUs are mounted on brackets of aluminum profiles screwed to a base frame. If unscrewed, the SPU frames can be shifted along the base frame. For the time-of-flight (ToF) measurements the SPU brackets have to be shifted to a positions marked on the base frame.
The radioactive ^{22}Na point source is mounted on a carriage adjustable in 3 dimensions (Figure 3.3). The movement along the axis between the two detector modules is controlled by a stepper motor connected to a raspberry pi computer. The datasheet of the ^{22}Na point source can be inspected at the day of the experiment.
The different components (DAPS, SPUs, backbone, stepper) are controlled via a system-control software (Hyperion) on a separate control-PC. An introduction to the system software will be provided by the tutor at the beginning of the lab day.

3.1.2 Power Supply and Cooling

Two DC power supplies provide 3 different voltages required to power the SPUs (Low 1.9 V, Mid 3.0 V, High 4.9 V) and the bias voltage of 30 V. The third power supply supplies on the first line a fan (12 V) cooling the electronics of the backbone and on the second line the stepper motor and its controller (24 V).
The electronics of the detector SPUs and sensor boards are cooled by water cooling driven by a transportable process thermostat (Lauda).

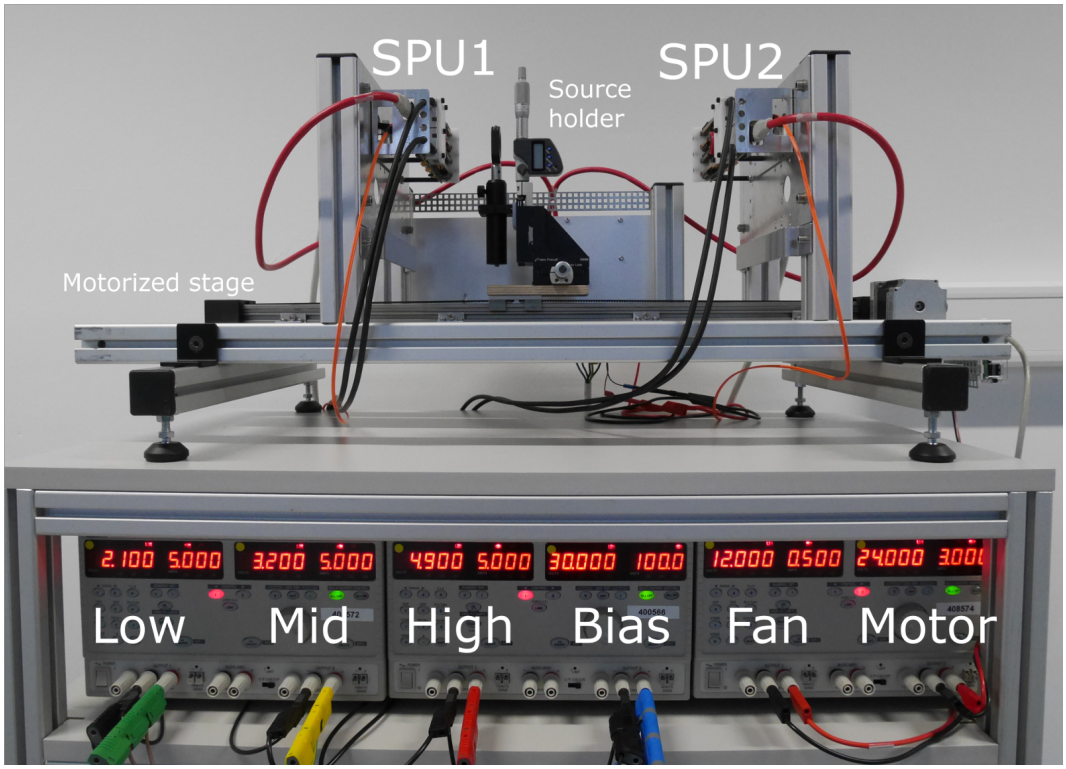

Figure 3.1: Setup of the Experiment, the backbone module is located behind the aluminum plate at the backside. The cooling unit, data acquisition and control PCs are not displayed.

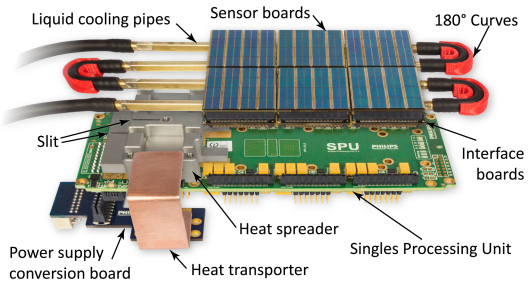

(a) Exploded-view photo of the SPU, detector stacks (without scintillator and light guide) and cooling infrastructure.

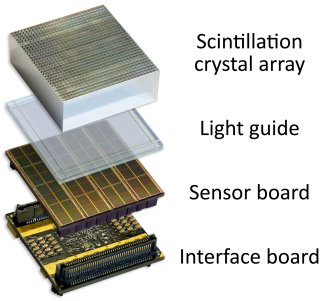

(b) dSiPM-based detector stack scintillation crystal array shown upside down to emphasize the individual crystals.

Figure 3.2: SPU and detector stack. Both images are taken from [8], CC BY 3.0 2015 IEEE

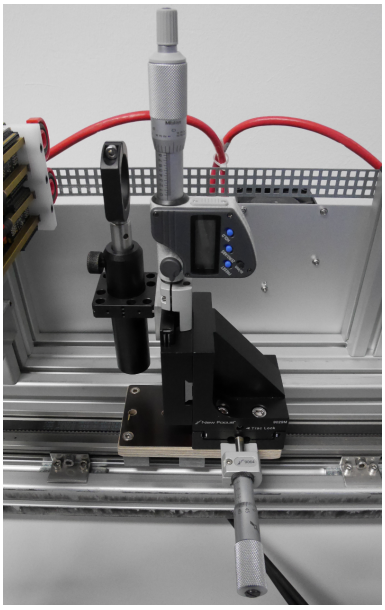

Figure 3.3: Source holder with translational stages to adjust the source's position. The holder is mounted to a motorized stage for movement between the detector modules.

3.1.3 Sensor board

The sensor boards are equipped with 16 sensor dies. Each of these dies has 2×2 dSiPM sensor channels that are connected via a single interface. The dSiPM-sensor channels (DLS 3200-22, Philips Digital Photon Counting, Aachen, Germany) consist of 3200 microcells, each with a size of $59.4\,\mu m \times 64\,\mu m$. Figure 3.4 shows the structure of sensor dies. The scintillator crystals for the experiment are currently under evaluation. Detailed information will be provided at the day of the experiment.

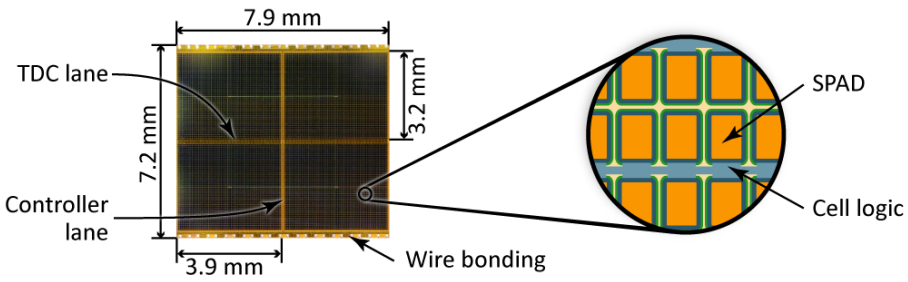

Figure 3.4: Microscopic photo of a monolithic 2×2 dSiPM array (left) with magnified sketch (right) of the sensor structure, from [9]

.

3.1.4 Start-up Procedure

The first start-up procedure should be performed together with the tutor.

Cooling Cooling should be started and running, before the SPUs are powered up. First power up the process thermostat and set the target temperature to 15 °C. Then power up the fan cooling the electronics of the backbone module. Check that the fan is rotating.

Power up the SPUs Switch on DC power supplies. Enable the three voltage supplying the SPUs from Low to High. At last switch on the bias voltage. In case a restart of the SPUs is required, switch off the voltages in reverse order (Bias first and subsequently High, Mid and Low). If the power up procedure of the SPUs is finished the blue status LEDs should switch off.

System Start-up procedure Start the Hyperion software and perform the start-up script. Check if the connection to the SPUs, the detector boards and the backbone are working by reading our their firmware versions.

Check temperatures Go to the control page and check the temperatures of the detector boards and SPUs. Wait until the sensor tile temperatures stabilizes and note down the measured temperature of all 4 sensor boards.

Finally power up the motor control computer (raspberry pi).

3.2 Procedure of the experiments

Since this experiment is currently in the development and testing phase the instructions are not finalized, yet. Detailed instructions for the acquisitions will be provided at the day of the experiment, at the latest. To save and copy your data for the analysis, please bring an USB-stick.

3.2.1 Determination of a dark count map

A dark count map is a plot of the individual dark count rates of the SPADS on a sensor board. To acquire such a dark count map, go to the configuration page and select the coincidence unit. In our case the coincident unit is the DAPS-PC which will control the acquisition. Select the entry 'spuDCM' in the commands field (in the lower right) to start the acquisition. The system will now measure the dark count rate for every SPAD and write it to a file. The control PC reports, when the measurement is finished and write the file to the hard disk. Check the file and save it to your USB-stick.

3.2.2 Count rate determination

Go to the status page of the control software and select the hit statistic entry. The count rate of singles and coincidences is displayed over time. Use the translational stages of the source holder and the stepper motor (via the control software) to move the source to the position with the maximum count rate of coincidences.
Start the measurement to save the count rate of singles and coincidences at the found position to determine an average value. Measure the distances from the source to the detector elements for later estimation of the geometrical sensitivity.

3.2.3 Energy spectrum

Go to the control page and select the energy spectrum entry on the left side. Energy histograms for singles and coincidences are displayed on the right side. Reset the histograms and start the measurement to acquire an energy histogram. After the acquisition is finished, save the histograms, check the files and copy them to your USB-stick.

3.2.4 Timing resolution and determination of source position by Time-of-Flight measurement

First the timing resolution of the detector is determined. To measure the timing resolution, acquire a histogram of time differences for the detected coincidences. Go to the control page and select the time resolution entry on the left side. Reset the measurement and restart it to collect and display the measured time differences. After the acquisition is finished, save the histogram and copy it to your USB-stick.
In the second part you should determine the unknown position of a point source by time-of-flight measurements. First move the brackets holding the SPUs on the base frame to the position with the label 'ToF'. Remember, that you have to loosen the screws at the bottom of the brackets a bit to move the them. Then, go the control page and select the entry: 'motor stage'. Select 'randomize position' to move the source to the new position. Then, go to the timing resolution page and acquire a new histogram of timing differences for the new position. Note, that you have to reset the measurement after moving the source to delete the entries measured at the old position.
Like before, save the histograms after the measurement, check the file and copy it to your USB-stick.

3.3 Analyzing your data

The data analysis can be done in an arbitrary program.

- Dark count map:
  - Plot the dark count maps in a suitable format.
  - Plot the overall dark count rate of the system against the fraction of inhibited SPADs with highest dark count rate.
- Sensitivity:
  - Calculate the average count rate of singles and coincidences and its uncertainty.
  - Compare the measured values to an estimation based on the geometrical sensitivity, scintillator dimensions and the activity of the source. In case you find significant differences, discuss by which effects they might be caused.
- Energy spectrum:
  - Plot the energy spectrum in a suitable way and label prominent points.
  - Determine the energy resolution of the PET-scanner and its uncertainty by fitting a Gaussian distribution to the 511 keV photo peak. Reason and discuss what data points you use for the fit.
  - Formulate and, if possible, test potential corrections to the data to improve the analysis. Discuss how the energy resolution of the system can be improved and what are the drawbacks of your suggested modifications.
  - Check the linearity of the energy calibration with the photo peak of ^{22}Na at 1275 keV. Formulate hypotheses why the energy scale might not be accurate at 1275 keV.
- Timing resolution:
  - Plot time difference histogram of the point source at central position in a suitable way and determine the coincidence resolving time (FWHM) of the PET system by fitting a Gaussian distribution to the time difference histogram.
  - Plot the time difference histogram for the unknown position. Both graphs can be combined to a single plot. Estimate the position of the point source from this measurements and make an estimation of the positions uncertainty.

Bibliography

[1] Versuch T1: Particle detectors and radiation protection, March 2015.

[2] Thomas Frach, Gordian Prescher, Carsten Degenhardt, Rik de Gruyter, Anja Schmitz, and Rob Ballizany. The digital silicon photomultiplier. In *2009 IEEE Nuclear Science Symposium Conference Record (NSS/MIC)*, pages 1959–1965. IEEE, 2009.

[3] H. Malcolm Hudson and Richard S. Larkin. Accelerated image reconstruction using ordered subsets of projection data. *IEEE transactions on medical imaging*, 13(4):601–609, 1994.

[4] Bernd Jähne. *Digital Image Processing*. Springer Science & Business Media, June 2013. Google-Books-ID: XczuCAAAQBAJ.

[5] David Schug. *About the calibration and PET performance of a preclinical PET/MRI insert equipped with digital silicon photomultipliers*. PhD thesis, RWTH Aachen, 2015.

[6] Lawrence A. Shepp and Yehuda Vardi. Maximum likelihood reconstruction for emission tomography. *IEEE transactions on medical imaging*, 1(2):113–122, 1982.

[7] Kenneth M. Tichauer, Yu Wang, Brian W. Pogue, and Jonathan T. C. Liu. Quantitative in vivo cell-surface receptor imaging in oncology: kinetic modeling and paired-agent principles from nuclear medicine and optical imaging. *Physics in Medicine and Biology*, 60(14):R239–269, July 2015.

[8] B. Weissler, P. Gebhardt, P. M. Dueppenbecker, J. Wehner, D. Schug, C. W. Lerche, B. Goldschmidt, A. Salomon, I. Verel, E. Heijman, M. Perkuhn, D. Heberling, R. M. Botnar, F. Kiessling, and V. Schulz. A Digital Preclinical PET/MRI Insert and Initial Results. *IEEE Transactions on Medical Imaging*, 34(11):2258–2270, November 2015.

[9] Bjoern Weissler. *Digital PET/MRI for preclinical applications*. PhD thesis, RWTH Aachen, 2016.

A Appendix

Na-22 decay scheme

22NA B+ DECAY http://atom.kaeri.re.kr/cgi-bin/decay?Na-22 EC

22NA B+ DECAY

Parent state: G.S.
Half life: 2.6088 Y(14)
Q(gs): 2842.0(5) keV
Branch ratio: 1.0

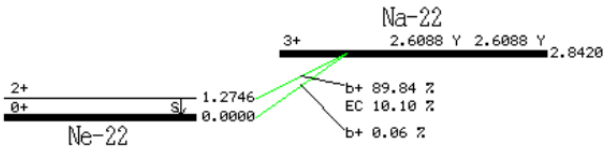

Beta+ ray: total intensity =89.9

Max.E(keV)	Avg.E(keV)	Intensity(rel)	Spin
1820.0(-)	835.00(23)	0.056(14)	3+
545.4(-)	215.54(21)	89.84(10)	0+
			2+

EC: total intensity = 10.1

Gamma ray:

Energy(keV)	Intensity(rel)
1274.53(2)	99.944(14)

P. M. ENDT, *Nuclear Physics* A521,1 (1990)

Please e-mail to *jhchang@kaeri.re.kr* for any comment. Thank you.

Figure A.1: Na-22 decay scheme from Korea Atomic Energy Research Center Institute: Table of Nuclides (http://atom.kaeri.re.kr)